MINISTRY OF EDUCATION AND TRAINING

HANOI UNIVERSITY OF MINING AND GEOLOGY

REPORT ON SCIENTIFIC SEMINAR

MODELLING THE BEHAVIOR OF A CIRCULAR TUNNEL IN TRANSVERSELY ISOTROPIC ROCK MASS

PRESENTER: Dr. BUI VAN BINH

DEPARTMENT OF ENGINEERING GEOLOGY

HANOI 12/2022

TABLE OF CONTENT

LIST OF FIGURE

LIST OF TABLE

ABSTRACT

In tunnel construction, tunnel stability is the most concern of any tunnel engineer. The factors such as geological condition, tectonic, excavation method, in-situ stress state, etc. The geological condition provides the necessary information about rock type, joint sets or weak planes as well as the geometrical and mechanical characteristics of joints or weak planes. The geological condition has an important role in design and construction of the tunnel. The effect of joint sets or weak planes on the tunnel stability has been studied by scientists. The tunnel stability in a transversely isotropic rock mass is a huge challenge due to the significant change of the mechanical properties under loading directions. Empirical guidance regarding tunnel stability reported in the literature indicated that the tunneling direction relative to joint strike and dip angle could affect the stability of a tunnel. However, little scientific data were available to quantify such an effect. This study aims to investigate the effect of joint orientation and dip angle through a series of three-dimensional (3-D) discrete element method (DEM) analyses that are set up to cover various tunneling scenarios. The synthetic rock mass simulated the transversely isotropic rock mass is generated by combining the intact rock model and Discrete Fracture Network (DFN) model. The intact rock model is created in Flow Particle Code software (FPC^{3D}) (Itasca 2014), whereas DFN model is generated in FracMan commercial software (FracMan 2011).The synthetic rock masses containing one joint set are generated with seven joint dip angles of 0°, 15°, 30°, 45°, 60°, 75° and 90°. Three tunneling scenarios were analyzed in synthetic rock mass: (1) Scenario I – tunneling direction parallel to joint strike, (2) Scenario II – tunnel axis perpendicular to joint strike and tunneling along dip direction, and Scenario III - tunnel axis perpendicular to joint strike and tunneling against the dip direction. These analyses covered diverse dip angles (β), ranging from 0° to 90° with an interval of 15°. The displacement, stress concentration, crack distribution and failure around the tunnel were analyzed. It is found that, for rock mass with low dip angles (β = 0°-15°), the tunnel stability is irrespective to the tunneling direction. It is rated “Fair” for the suitability for tunneling. For rock mass with dip angles of 45°- 60°, terrible displacement and severe failure is observed in the tunnel under Scenario I, while effects under Scenario II and Scenario III are less severe. The displacement around the tunnel under Scenario III is

much more than that under Scenario II. For rock mass with high dip angles (β = 75°-90°), the grade of tunnel stability under Scenario II and Scenario III is rated "very favorable," whereas the grade under Scenario I is found "favorable." From the numerical experimentation, a slight modification to Bieniawski's classification rule is proposed.

Otherwise, from the displacement vectors of rock blocks around the tunnel, four displacement field types are proposed to describe the damage process and damage state of rock mass around the tunnel. Tensile displacement field with the joint (DF-I) represents the detachment of the rock layer around the joints. Tensile displacement field in intact rock (DF-II) describes the slabbing phenomenon of rock mass in the slabs in the sidewall of the tunnel. Shear and tensile displacement field (DF-III) and shear displacement field type (DF-IV) delineates the tendency to the sliding movement of rock mass along the joint into the tunnel. In addition, failure modes around the tunnel corresponding to each scenario are presented in this study. Scenario I reports four failure modes such as "Detaching and Buckling," "Sliding," "Bending and Spalling," and "Slabbing and Spalling." In Scenario II and Scenario III, "Bending and spalling" mode is observed in the crown and invert of the tunnel. "Slabbing and Spalling" occurs in the sidewall. "Detaching and Buckling" occurs in the tunnel face with rock mass containing vertical joint set. In the tunnel face under Scenario II, "Falling" mode is observed with dip angles of 30°- 75°, whereas "Sliding" model is shown with dip angles of 30°- 75° in the tunnel face under Scenario III. Although the findings of this study are considered preliminary and with several limitations, it provides insight into the effect of tunneling direction on tunnel stability in a transversely isotropic rock mass.

1. INTRODUCTION

1.1. Transversely isotropic rock mass

In rock engineering practice, the determination of reasonable mechanical parameters of rock and rock mass is a significant challenge governing the design and constructive schedule of any project. Formed in nature and governed by complicated geological processes, rock and rock mass always show the elastic and strength anisotropy. In the past, many authors dedicated their efforts to elucidate the strength anisotropy as well as failure criteria of transversely isotropic rock. Based on the single weakness plane theory, Jaeger., 1960 proposed the failure criterion with two independent failure modes: failure along the discontinuity and failure cross intact rock. His study showed that the strength of transversely isotropic rock varies with inclination angles (β). Liao et al., 1997 investigated the direct tensile behavior of argillite rock under direct tensile tests. Tien and Kuo., 2001 proposed a new failure criterion for the transversely isotropic rocks based on two distinct failure modes as sliding along the discontinuity and non-sliding, in which the failure is governed by the rock material. Lee and Pietruszczak., 2008 under the assumption of the Hoek-Brown criterion governing the initiation of cracking, authors proposed the formulation to estimate the strength isotropy of transversely isotropic rock using the critical plane approach. Ghazvinian et al., 2013 examined the effect of schistosity plane orientation on the failure mechanism and the shear behavior of anisotropic rock. Vervoort et al., 2014 investigated the behavior of transversely isotropic rock under Brazilian tests. Lee and Pietruszczak., 2015 proposed a 3-D tensile failure criterion for transversely isotropic rock in which the failure condition involves three strength parameters and employs a second-order tensor to describe the spatial distribution of the tensile strength.

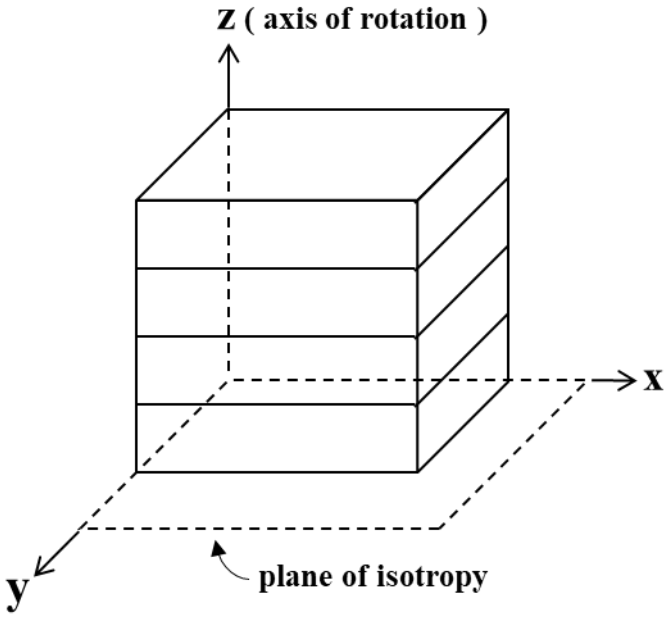

Figure 1.1. Conceptual model of transversely isotropic material

$$\begin{bmatrix} \varepsilon_x \\ \varepsilon_y \\ \varepsilon_z \\ \gamma_{yz} \\ \gamma_{xz} \\ \gamma_{xy} \end{bmatrix} = \begin{bmatrix} \frac{1}{E} & \frac{-\nu}{E} & \frac{-\nu'}{E'} & 0 & 0 & 0 \\ & \frac{1}{E} & \frac{-\nu'}{E'} & 0 & 0 & 0 \\ & & \frac{1}{E'} & 0 & 0 & 0 \\ & \textit{symm.} & & \frac{1}{G'} & 0 & 0 \\ & & & & \frac{1}{G'} & 0 \\ & & & & & \frac{1}{G} \end{bmatrix} \times \begin{bmatrix} \sigma_x \\ \sigma_y \\ \sigma_z \\ \tau_{yz} \\ \tau_{xz} \\ \tau_{xy} \end{bmatrix}$$

Recently, with the development of computational mechanics, the Discrete Element Method (DEM) is used to investigate the mechanical behavior of rock mass. It showed the effectiveness in simulating the progressive failure of rock. Potyondy and Cundall., 2004 proposed a bonded-particle model for rock in which rock is represented by dense-packing of non-uniform-sized circular or spherical particles that are bonded together at their contact points. More recently, many investigators have combined the bonded-particle model and smooth joint model to investigate the mechanical behavior and the failure mechanism of complicated material such as synthetic rock mass or fractured rock mass. Most of them focused on the 2-D model; in fact, very few authors used the 3-D model with the assumption of fractures being persistent.

Park et al., 2015&2018 used the two-dimensional and three-dimensional bonded-particle discrete element method and smooth joint model to simulate the mechanical behavior of transversely isotropic rock. From the comparison between the numerical results and laboratory observations on three rock types (gneiss, shale, and schist), it showed the reasonable agreements to estimate the elastic and strength parameters of transversely isotropic rock. Pouragha et al., 2020 studied the correlation between macroscopic elasticity and strength characteristics of transversely isotropic rock and proposed an analytical procedure to estimate the rock strength anisotropy.

It is challenging to estimate the strength anisotropy of rock mass with a direct full scale in rock engineering practice, as the information on fracture characteristics obtained from field investigation almost always contains uncertainties. Thus, it is difficult to ascertain the design parameters. In this paper, we combine the three-dimension bonded-particle discrete element method and smooth joint model to simulate the fractured transversely isotropic rock mass, in which fractures are generated randomly based on the distribution of the geometrical parameters of the fracture. The effects of geometrical parameters of the fracture on the mechanical behavior are also examined.

1.2. How to modeling the Synthetic rock mass

A Synthetic Rock Mass (SRM) model is referred as a numerical medium for the simulation of the jointed rock mass response involving the construction and testing works. The SRM is composed of the intact rock model and the systematic fracture sets that is referred as a Discrete Fracture Network (DFN) (Pierce et al. 2007). So, the SRM model is adopted to simulate the huge rock volumes containing a vast number of joints (Pierce et al. 2007, Sainsbury et al. 2008, Esmaieli et al. 2010, Ivars et al. 2011, Harthong et al. 2012, Farahmand et al. 2018). The mechanical behavior of the SRM is considerable governed by the behavior of the intact rock as well as the mechanical and geometrical properties of the DFN model.

The intact rock is referred as the rock blocks which lie among the discontinuities. On the other hand, it is also known as a rock score or rock sample using in the experimental tests (laboratory tests). Several scholars made the assumption that rock behaves like a assemble of bonded particles (Cundall et al. 1982, Potyondy et al. 1996,

Potyondy and Cundall 2004). In the past, the rock was simulated by bonded assemblies of circular particles (Potyondy et al. 1996). The behavior of the rock depends on the characteristics of the cement material which bonds the particles together. The simulation of the mechanical characteristics of the cement material is a challenging task. Potyondy and Cundall (2004) proposed a numerical model that the rock is described by a dense packing of circular or spherical particles, in which particles are bonded together at their contact points. This numerical model is referred as the bonded-particle model (BPM). The model would replicate almost characteristics of intact rock behavior involving strength, elasticity, fracturing, acoustic emission (Potyondy and Cundall (2004), Pierce et al. 2007). The BPM has been popularly adopted to simulate the mechanical behavior of the intact rock (Yoon 2007, Pierce et al. 2007, Esmaieli et al. 2010, Ivars et al. 2011, Park and Min 2015, Farahmand et al. 2018, Ma and Huang 2018)

A Discrete Fracture Network (DFN) seems to a computational model describing the geometrical characteristics of the fracture (i.e., position, size, orientation and aperture) as well as the relationship between fracture sets and individual fractures (Lei et al. 2017). The DFN is one of the key components to create the synthetic rock mass model. Initially, the stochastic modelling of fracture networks mentioned in previous studies (Robinson 1983, Sahimi 1993). The application of the stochastic fracture network model to rock engineering was promoted in the late 1980s by several scholar's work (Long et al. 1982, Baecher 1983, Dershowitz and Einstein 1988). The characteristics of fracture networks as orientation, size, location and other parameters are treated as random variables of adopted probability distributions (Xu and Dowd 2010). To simplified the problem, the geometry of fractures is assumed with the straight line for two dimensional model (2D) and disk or ellipse for three dimensional model (3D). The characteristics of fracture networks as size, orientations, fracture intensity as well as the adopted probability distribution would be used to construct the stochastic fracture network model. These characteristics of fracture networks are obtained by the field measurements from outcrop scanline, window mapping, borehole logging, and rock surface extraction (tunnel, ditch and open pit) (Xu and Dowd 2010, Ivars et al. 2011). Recently, the DFN model has been popularly used to model the synthetic rock mass (SRM) (Pierce et al. 2007, Esmaieli et al. 2010, Xu and Dowd 2010, Ivars et al. 2011, Harthong et al. 2012, Lambert and Coll 2014). The DFN model plays an important

role in reproduce the realistic synthetic rock mass from the field geological data. It helps scholars investigate the mechanical behaviors of complex rock masses and provide further understanding of complex responses of rock mass in construction field.

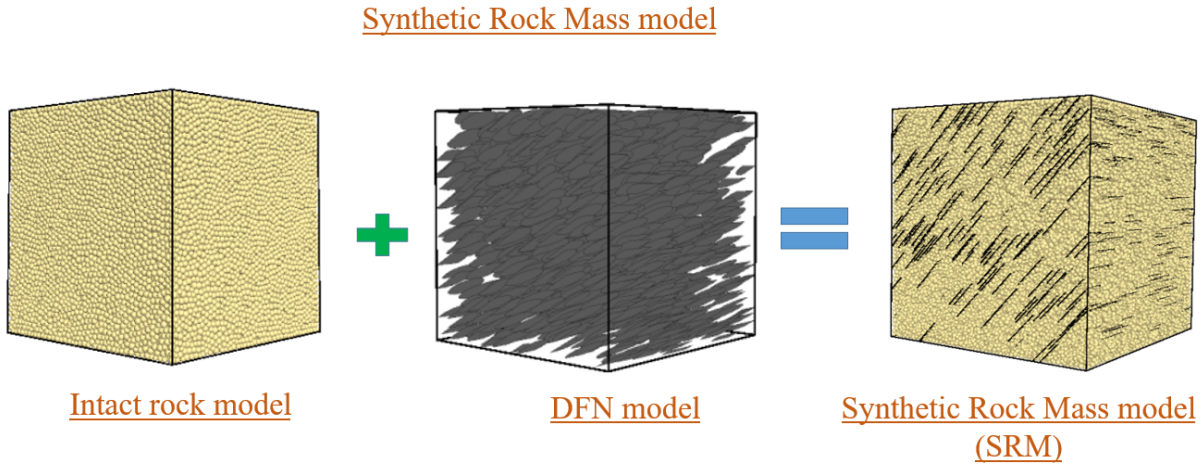

Figure 1.2. Synthetic rock mass model

1.3. Introduction to tunnel in transversely isotropic rock mass

The tunnel construction activity in a transversely isotropic rock mass always poses a real challenge to tunneling engineers due to its important features of strength and elastic anisotropy. The behavior of rock mass around the tunnel is strongly controlled by the orientation of bedding planes or joint sets. Sufficient knowledge about the effect of joint orientation on tunnel stability is of importance in the planning of geotechnical investigation and construction of the tunnel. This study investigates the influence of joint dip angle on the displacement distribution around the tunnel in the transversely isotropic rock mass by using the three-dimensional Particle Flow Code (PFC3D). The case of the tunnel direction parallel to joint strike is focused on studying.

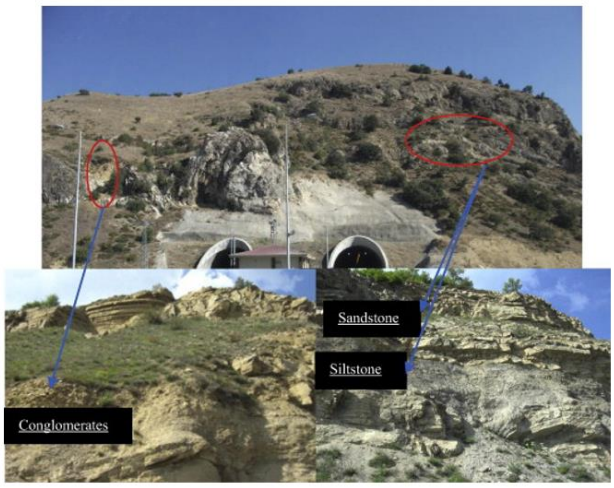

Tunneling in a transversely isotropic rock mass
Satıcı and Ünver (2015)

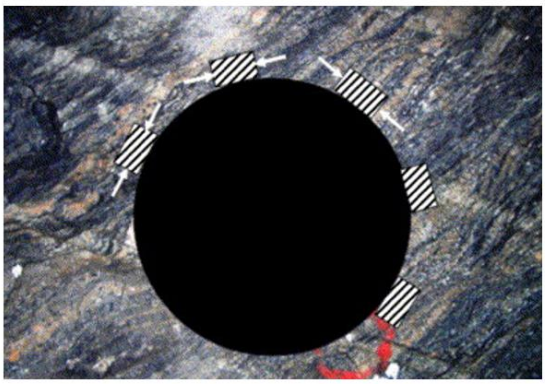

Tien et al. (2006)

Figure 1.3. Tunnel in transversely isotropic rock mass.

Many scientists have made a tremendous effort to elucidate the role of joint orientation, dip angle, joint spacing, field stress state, tunnel direction, etc., in tunnel construction. Wickham et al., 1972; Bieniawski, 1974, 1989 quantified the influence of joint orientation concerning tunnel direction on tunnel stability.

Obert and Duvall, 1967; Jaeger and Cook, 1979 investigated the stress redistribution around the tunnel in a transversely isotropic rock mass under uniaxial stress state conditions. They showed that the effects of strength anisotropy were more important than the effects of elastic anisotropy.

The development of the numerical method has helped scholars conduct the ideas with low expenditure. Wittke, 1990; Tonon and Amadei, 2003 researched the stress redistribution and displacement around the unsupported tunnel in a transversely isotropic rock mass using Finite Element Method (FEM). In addition, Klopčič and Logar, 2014 studied the share of displacement and the extent of influence zone distributing ahead and behind the tunnel face when excavation in the transversely isotropic rock mass.

More recently, some investigators focused on the cracking initiation, propagation, and failure mechanism around the tunnel in an anisotropic rock mass. Jia and Tang, 2008 studied the effect of dip angles (β = 0°, 30°, 45° and 60°) and the lateral pressure coefficient on the stability of the tunnel in the jointed rock mass by the numerical code Realistic Failure Process Analysis ($RFPA^{2D}$). They indicated that the failure mode was the breakage of a rock beam in a rock mass with horizontal layers. For mild dip angles of 30° and 45°, the sliding of joint and the detachment and breakage of the layered rock mass occurred. For the high dip angle, the overall sliding failure of the rock mass occurred along with the interface of joints. Wang et al., 2012 focused on the failure mechanism for a circular tunnel in the transversely isotropic rock under uniaxial and biaxial compressions by using the $RFPA^{2D}$ code. The rock-tested models had the laminated layers with dip angles such as 0°, 15°, 30°, 35°, 60°, 75°, and 90°. They showed that for dip angles of 0°, 15° and 30°, the failure process of the tunnel in a transversely isotropic rock mass under uniaxial loading was controlled by tensile cracking. For dip angles of 45°, 60° and 75°, the failure was mainly caused by shear

stresses. Finally, the laminated layers with lower stiffness and strength lost their ability to support load due to the effects of tensile cracking with dip angle of 90°.

More recently, the Discrete Element Method (DEM) has significantly developed. The particle flow code (PFC) has popularly used in simulating the crack propagation of the material. Sagong et al., 2011 researched the rock fracture and joint sliding behavior of a jointed rock mass with a hole under biaxial compressive condition. Cao et al., 2018; X. Yang et al., 2016 and S.-Q. Yang et al., 2019 investigated the crack evolution mechanism of a non-persistent jointed rock mass containing a circular hole under uniaxial compression by the experiment and numerical simulation (PFC^{2D}). The results indicated that the strength and elastic behavior of the specimen with respect to joint inclination displayed a U-type. The crack coalescence modes between the circular hole and its adjacent joints were controlled by dip angles of the joint set.

This study focuses on studying the effect of joint dip angle on the displacement distribution around the tunnel in a non-persistent jointed rock mass by the three-dimensional bonded-particle discrete element method (PFC^{3D}). The joint's dip angles were created from 0° to 90° with an interval of 15°. Otherwise, the three-dimensional stress state was used to simulate the stress state of the rock mass model. This allows us to simulate the stress redistribution and displacement distribution around the tunnel during excavation more accurately. This study provides a comprehensive view of the effect of joint dip angle on displacement distribution and failure modes around the tunnel when tunnel direction is parallel to joint strike.

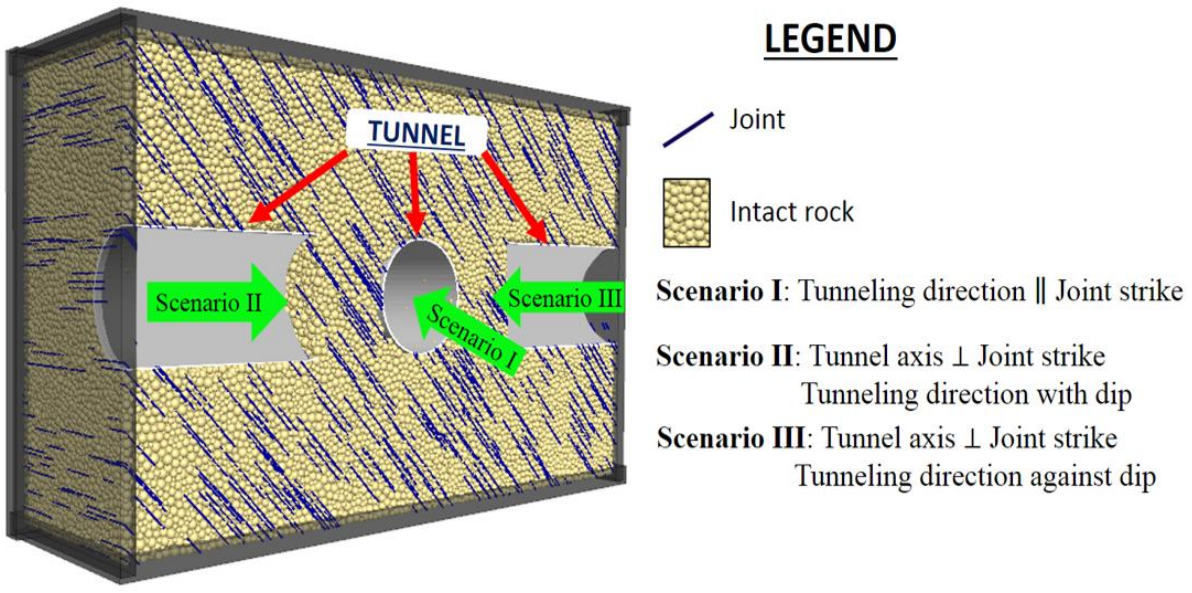

Figure 1.4. Conceptual model of tunneling in a transversely isotropic rock mass

2. METHODOLOGY

2.1. Intact rock model

Intact rock is referred to as an unfractured block among discontinuities in a general rock mass. The laboratory is a specimen of any rock type to determine the strength and elastic properties. In numerical analysis, the intact rock is generated to simulate any rock type's real behavior in nature. It is also a principal part of the complicated model as a synthetic rock mass in the numerical model. In this study, the intact rock is generated by the commercial PFC3D software (*Itasca Consulting Group Inc. 2014*) with a bonded-particle model (BPM) proposed by Potyondy and Cundall, 2004. The BPM is a conceptual assembly of non-uniformed-sized spherical particles. The particles are bonded at their contact points. In the BPM the particles are the rigid and non-deformed balls and joined at the contact by a glue substance called "contact bond." [10] The mechanical behavior of intact rock depends on the micro-parameters of the contact model assigned to contact points. The breakage of the contact bonds would occur when the applied force exceeds its strength. The force and moment at the contact bond are updated after every calculation cycle. Newton's second law and force-displacement law are used to calculate the force and movement after every calculation cycle [10]. In the present study, the linear parallel bond model is assigned to all ball-ball contact points. The parallel bond describes the mechanical behavior of a finite-sized piece of glue material distributed between the two contacting pieces. The linear parallel bond consists of the parallel-bond and linear components. They act simultaneously and establish an elastic interaction between the pieces. Both force and moment between the pieces can be transmitted by parallel bonds. The micro-parameters of the linear parallel bond model are shown in Table 1.

Table 1. Micro-parameters of the linear parallel bond model

Micro-mechanical parameters	**Values**
Particle density, (kg/m^3)	2650
Porosity, ρ	0.2
Minimum particle radius (m)	0.133

Particle radius ratio, R_{max}/R_{min}	1.5
Particle contact modulus, E^* (GPa)	20.5
Particle normal to shear stiffness ratio, k_n/k_s	3.0
Particle friction coefficient, μ	0.50
Parallel-bond radius multiplier, λ	1.0
Parallel-bond effective modulus, $\bar{E}^*$ (GPa)	20.5
Bond normal to shear stiffness ratio, $\bar{k}_n/\bar{k}_s$	3.0
Tensile strength, $\bar{\sigma}_c$ (MPa)	15.0
Cohesion, $\bar{c}$ (MPa)	35.0
Friction angle (degree)	0

The uniaxial compressive test is conducted to determine the mechanical behavior of the intact rock model. The fifteen rectangular prism samples of the intact rock with the size of 1.5 m × 1.5 m × 3.0 m are generated to carry out the uniaxial compressive test. The stress-strain curve is shown in Fig. 1. The uniaxial compressive strength (σ_c) of intact rock is 67.9 MPa, while Young's modulus (E_{50}) is 35.9 GPa. The Poisson's ratio (ν) is 0.22.

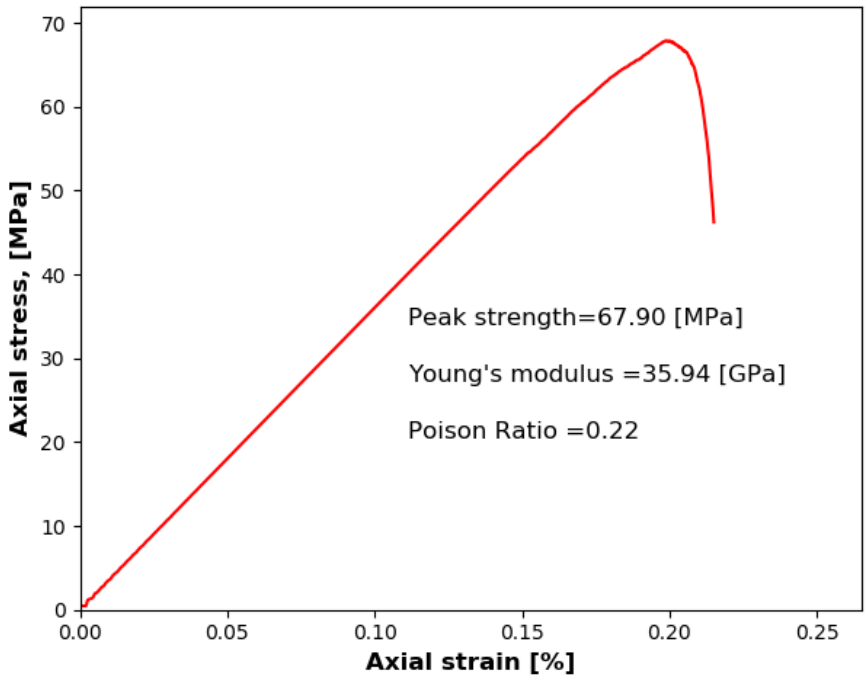

Figure. 2.1. Stress-strain curve of intact rock model under uniaxial compressive test.

2.2. Discrete fracture network model

The Discrete Fracture Network (DFN) model expresses the geometrical relationships between fractures, fracture sets, and each fracture [8]. The DFN model is an assemble of fractures or fracture sets. This model helps authors create the approximate fracture sets from the characteristics of fracture sets measured at the site. In the present study, the commercial FracMan software (*Golder Associates, 2011*) is used to create the DFN model. Because the study focuses on the transversely isotropic rock mass, one joint set containing the parallel joints is created. The geometrical parameters of the joint set, such as joint orientation (dip direction, dip angle), orientation distribution, fracture intensity, size of fractures, are used to generate the DFN model [4]. Because the shape of fractures in the DFN model is assumed like a circular disk, the terminology of the fracture diameter (D) will be used instead of the fracture size.

In this study, the DFN model containing one joint set is generated with fracture intensity (P_{32}) of 1 m^2/m^3, fracture diameter (D) of 15m. To generate the joint set containing the parallel joints, the Fisher distribution with Fisher constant (κ) of infinity is adopted to depict the orientation distribution of the joints. Seven DFN models with joint dip angles of 0°, 15°, 30°, 60°, 75° and 90° are generated. The mean of joint spacing in all models is rough 1.0m. The size of the DFN model is $30 \times 35 \times 35$ m^3.

2.3. Synthetic rock mass model

Synthetic rock mass represents the complex media containing the matrix rock and geological structures. In numerical analysis, the synthetic rock mass is a combination of the intact rock model and DFN model. So, the behavior of synthetic rock mass depends on the mechanical behavior of both intact rock and fractures in the DFN model. To simulate the mechanical behavior of the fractures in the DFN model, the smooth-joint contact model is assigned to the contacts of the pair of the particles lying on the opposite sides of the joints. The smooth-joint model provides the macroscopically mechanical behavior of a linear elastic and frictional planar interface [10]. The shear force is updated after every calculation cycle. When shear force at the smooth-joint contacts exceeds the bond shear strength, sliding occurs. The mechanical behavior of the joints depends on

the micro-mechanical parameters of the smooth-joint model as normal stiffness (sk_n), shear stiffness (sk_s), and friction coefficient (μ). These micro-parameters are changed in the trial process by the direct shear test so as to get the approximate real behavior of the joint, called "trial and error" method. The micro-mechanical parameters of the smooth-joint model are indicated in table 2.

Table 2. Micro-parameters of the smooth joint model

Micro-mechanical parameters	Values
Normal stiffness per unit area, sk_n (N/m/m^2)	5.63×10^9
Shear stiffness per unit area, sk_s (N/m/m^2)	1.05×10^9
Joint cohesion, c	0.0
Joint friction coefficient, μ	0.50
Joint tensile strength, σ_c (MPa)	0.0
Large strain flag	1

By combining the intact rock model and DFN model with the smooth-joint contact model representing the contacts between the particles lying on opposite sides of the joint, the synthetic rock mass is created. Seven synthetic rock masses corresponding to seven joint dip angles of 0°, 15°, 30°, 45°, 60°, 75° and 90° are generated. The size of the synthetic rock mass is 30m × 35m × 35m. The anisotropic strength and elastic behaviors of the synthetic rock mass are investigated by a uniaxial compressive test. Fifteen samples for each joint dip angle with the size of 3m × 3m × 6m are randomly taken from the synthetic rock mass. The relationship between strength and elastic behavior and dip angles of the synthetic rock mass is illustrated in Fig. 2.2.

Fig. 2.2 showed that the mechanical behavior of the synthetic rock mass is governed by the joint dip angles. The curve of the uniaxial compressive strength and the dip angle has a "U-type." With dip angles of 30° - 60°, the strength of the rock mass is minimum. The maximum strength is indicated with the dip angle of 90° (vertical joint). The sample with horizontal joints showed the second maximum strength. The ratio of the strength between the vertical and horizontal joint is 1.5. The relationship between Young's

modulus and dip angle shows a similar trend with the strength. The ratio of Young's modulus of $\beta = 90°$ and that of $\beta = 0°$ is 2.78.

2.4. Tunneling procedure and measurement systems

Before performing the tunnel construction, the synthetic rock mass is applied to the three-dimensional stress state. The major principal stress (σ_1) is the vertical stress, while intermediate and minor principal stress (σ_2, σ_3) are the horizontal stress with σ_2 parallel to the tunnel axis. The value of major principal stress is 20 MPa, and intermediate and minor principal stress are 10 MPa. These stresses are applied to the boundary of the synthetic rock mass model. They are increased gradually, and the similar increasing stress rate of three directions is applied. When the horizontal stresses reach the aim value, they are kept constant, whereas the vertical stress continues gradually increasing to the target value of 20 MPa before remaining unchanged. After all the stress boundary conditions approach the expected stress state, the bottom plane of the model is fixed with the non-displacement condition, as illustrated in Fig. 2.3. The excavation process is initiated. The tunnel has a circular shape with a diameter of 8 m. The length of the tunnel is 15 m, half of the length of the model. The tunneling process is excavated with six steps. The excavation length of each step is 2.5 m, as shown in Fig. 2.4. In each step, all particles falling into the extent of the appropriate step are deleted simultaneously. The full-face excavation method without the support installation is applied. In each step, a certain number of cycles are run in the order that the model reaches the equilibrium state before the next step is excavated.

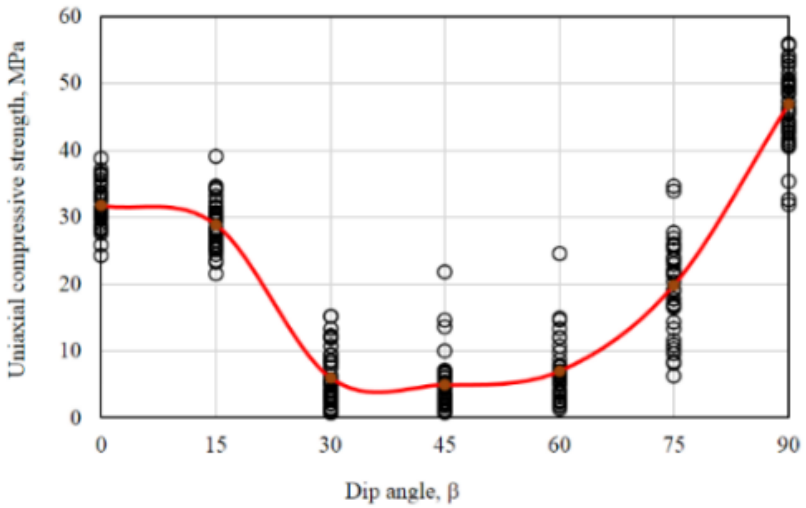

(a)

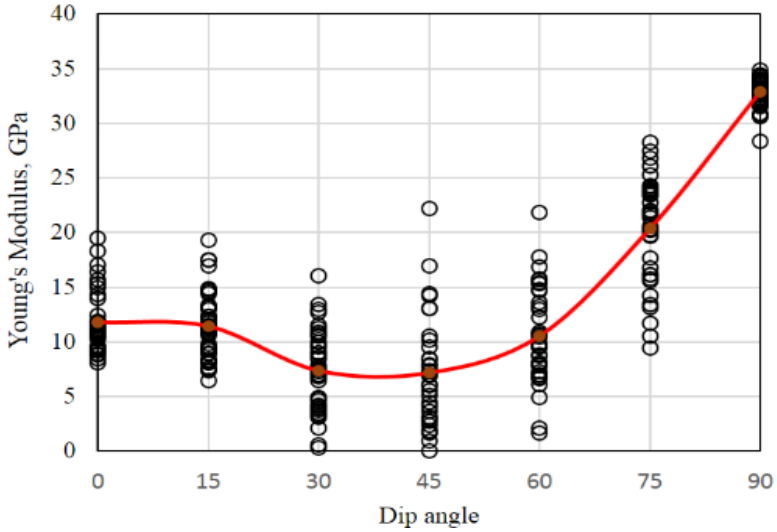

(b)

Fig. 2.2. The relationship between the mechanical behavior and dip angle: (a) uniaxial compressive strength; (b) Young's modulus

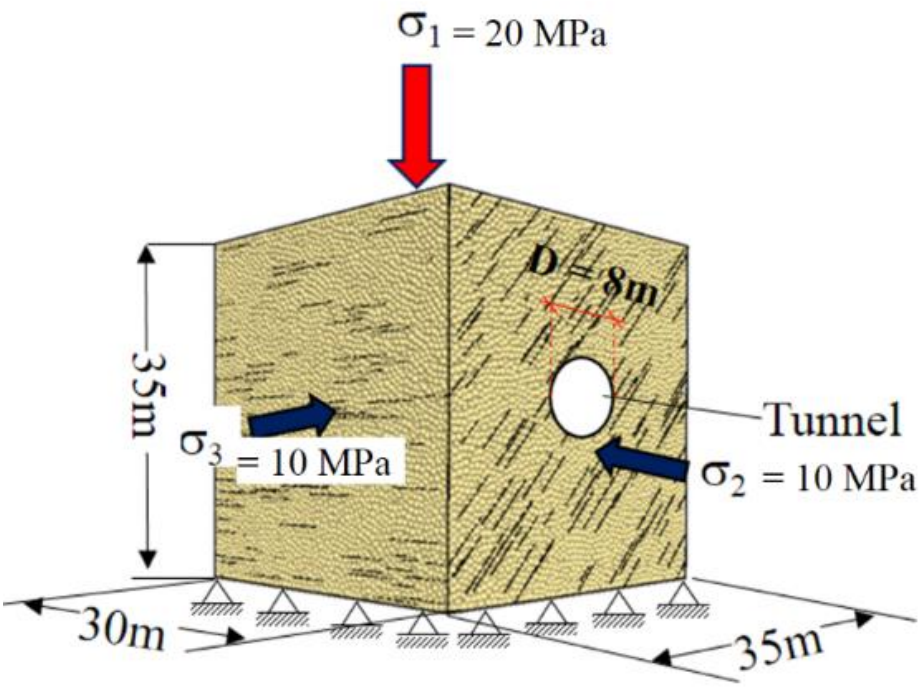

Figure. 2.3. Model of tunneling in the anisotropic rock mass

In this study, the case of the tunnel direction parallel to joint strike is simulated as mentioned above. Seven transversely isotropic rock masses corresponding to seven joint dip angles (i.e., 0°, 15°, 30°, 45°, 60°, 75°, and 90°) are used to investigate the effect of dip angle on displacement distribution around the tunnel.

The stress and displacement around the tunnel are measured by a measurement system, including stress and displacement gauges along the tunnel and two cross-sections of C1 and C2, as shown in Fig. 2.4. Each stress gauge is a spherical volume with a radius of 0.5 m. It measures the average of stress at all contact points containing in it. Each displacement gauge is assigned to a particle at a certain position. The movement of the chosen particle compared to its original position after every cycle is the displacement. The cross-section C2 is set at the final tunnel face, while the C1 is set far from the tunnel face of 8 m, as shown in Fig. 2.4a. The gauges are arranged along the tunnel and two cross-sections with a space of 2.0 m. Otherwise, to mitigate the effect of the local failure on the tunnel periphery, the gauges are set at the nearest points (i.e., 1.0 m) from the tunnel boundary. In this study, the radial displacement presents the displacement around the tunnel.

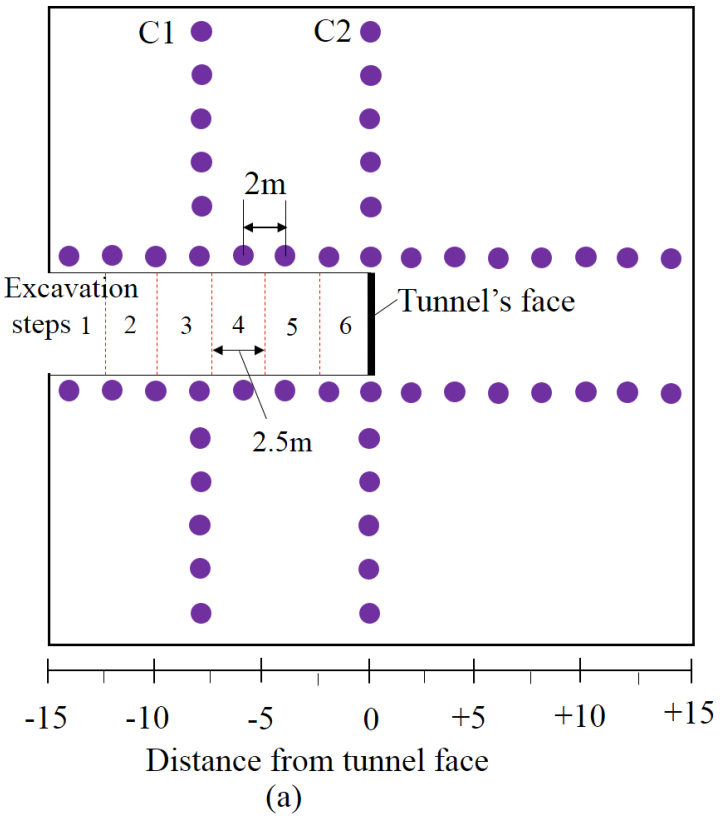

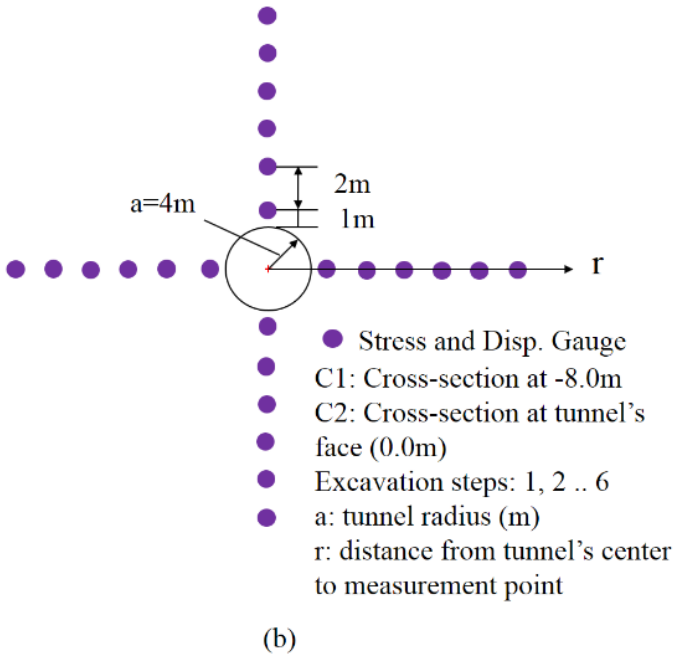

Figure.2.4. Measurement system: (a) along the tunnel axis; (b) at cross-section perpendicular to the tunnel axis

3. NUMERICAL ANALYSIS

3.1. Behavior of transversely isotropic rock mass under uniaxial compression loading

To investigate the mechanical behavior of fractured transversely isotropic rock mass, we performed the numerical simulations of uniaxial compressive tests. The parameters considered include the sample size of $1.5 \times 1.5 \times 3$ m^3, fracture diameter (D) of 2 m, fracture intensity (P_{32}) of 1 m^{-1}, Fisher constant (κ) of infinity and different inclination angles, β of 0˚, 15˚, 30˚, 45˚, 60˚, 75˚ and 90˚. To eliminate or reduce the assessment bias, we used thirty random samples of fractured rock mass for each inclination angle. The numerical results showed that the elastic and strength anisotropy of fractured rock mass significantly changes with the different inclination angles. The change of uniaxial compressive strength and Young's modulus with varying angles of inclination may be as a U-shape, as shown in Figure 3.1. It is seen from Figure 3.1 that samples with the inclination angle (β) of 0° and 90˚ exhibit the highest mechanical properties with small variations. Whereas samples with β = 30° and 45˚ approach to the lowest values of mechanical properties. These results agreed well with those of Tien et al., 2006.

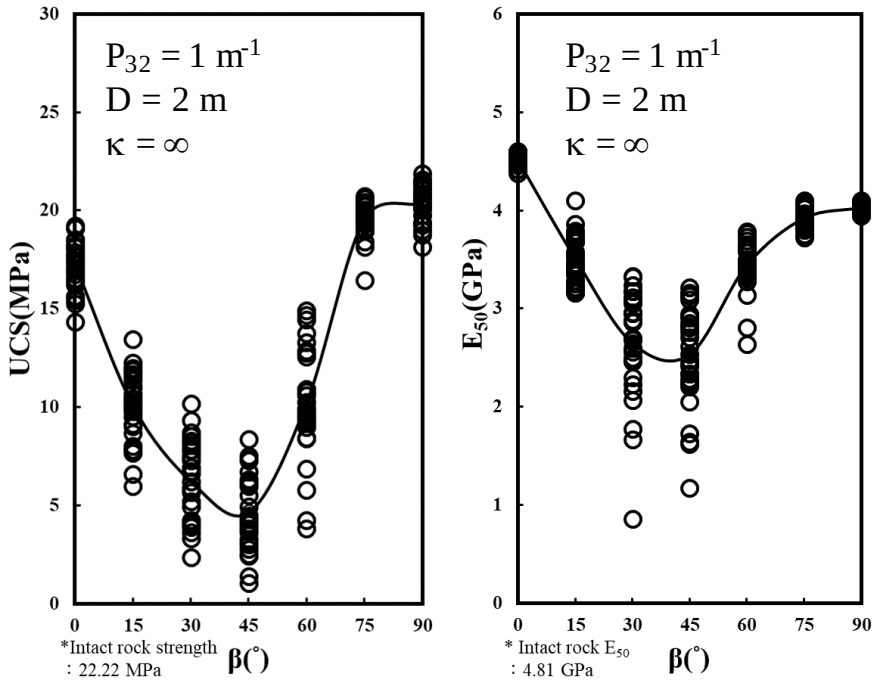

Figure 3.1. Effect of dip angle on the mechanical properties: (a) uniaxial compressive strength, (b) Young's modulus

From the cracking propagation and failure modes of rock mass during testing with varying inclined angles, the failure modes of fractured transversely isotropic rock mass under the compression loading can be divided into four types in the following. First, Sliding or Split across the fracture mode (SS): New cracks develop in intact rock and then blend to form the failure plane. The failure plane direction is relatively orthogonal to inherent fractures. Such damage is slightly affected by the inherent fractures and is more likely to occur at inclination angles of $\beta = 75^{\circ}$ and 90°. The relationship between the failure process and applied loading is plotted in Figure 3.2. Second, Sliding along the inherent fracture mode (SL): The new cracks develop in parallel with the direction of the inherent fractures. The cracks are gradually generated and connected to the inherent fractures to form the failure plane, as shown in Figure 3.3. This mode mostly occurs with inclination angles $\beta = 15^{\circ}$, 30°, 45°, and 60°. Third, Split along the inherent fracture mode (SP): The new cracks fully develop in intact rock. Due to the inherent vertical fractures, cracking orientation is controlled by the inherent vertical fractures. Consequently, the failure occurs by splitting along the inherent fractures. This mode easily occurs with an inclination angle of $\beta = 0°$. Fourth, Mixed mode (M): when sliding and penetrating or sliding and splitting failure modes coexist, it is said to occur in fractured rock masses with dip angles of $\beta = 15^{\circ}$ and 75°. The numerical simulation results are very similar to the experimental observations of Tien et al., 2006 and Cho et al., 2012, as shown in Figure 3.4.

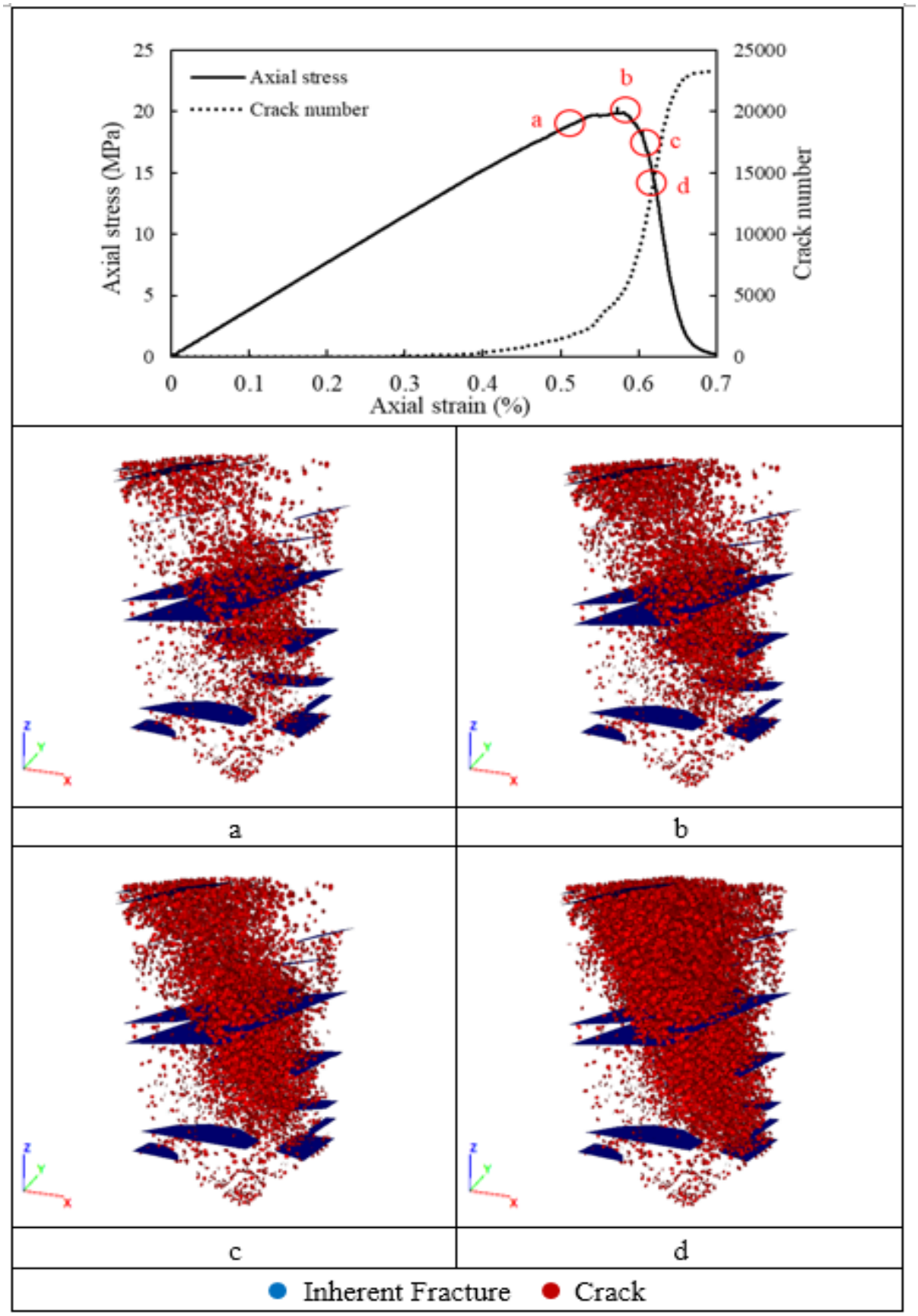

Figure 3.2. Cracking propagation corresponding to the applied loading of the SS model.

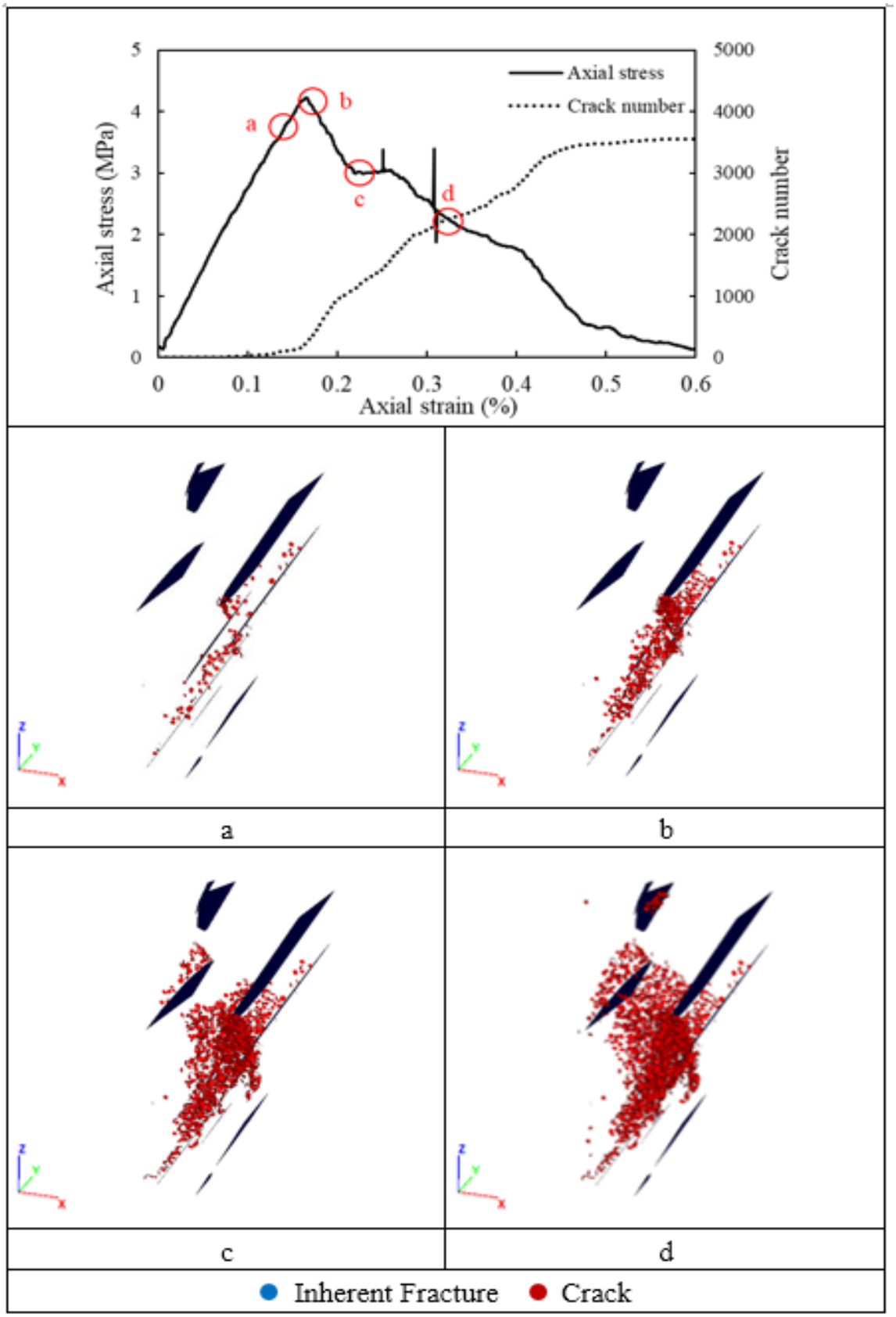

Figure 3.3. Cracking propagation corresponding to applied loading of SL mode.

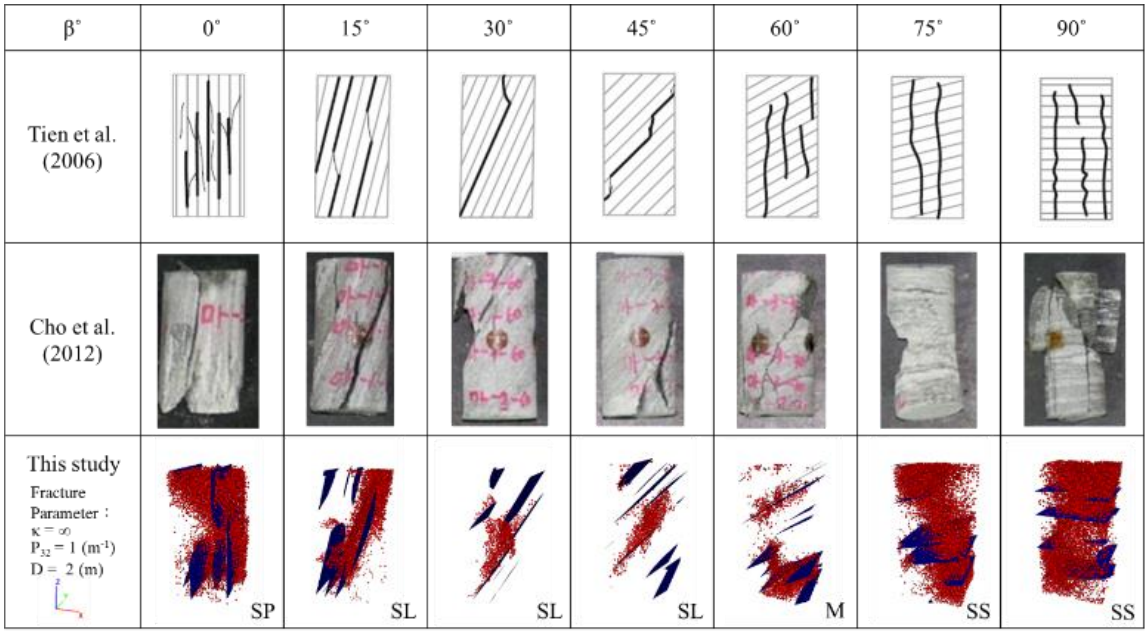

Figure 3.4. Comparison of failure modes of this study with Tien et al., 2006 and Cho et al., 2012

3.2. Effect of dip angle on displacement

In tunneling construction, the distribution of stress and displacement around the tunnel is a key parameter to assess tunnel stability. Due to the effect of the excavation process caused the stress distribution around the tunnel, the displacement occurs. The closer the tunnel boundary, the larger the displacement. The displacement majorly distributes in the crown and invert the tunnel, whereas it is relatively small at the sidewalls. Fig.3.5 shows the displacement at the crown and the right sidewall of the tunnel corresponding to the excavation steps at the dip angle of 45°. Before excavating, the displacements along the tunnel axis are approximately zero. They increase gradually, corresponding to each excavation step. The blue line shows the displacement along the tunnel of step 6, the final excavation step. It shows that behind the tunnel face, the farther the tunnel face, the larger the displacement. The displacement at the crown was much more than that at the right sidewall.

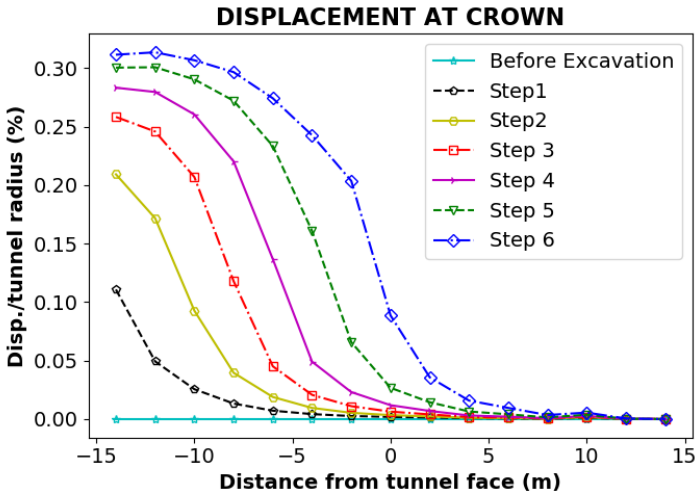

(a)

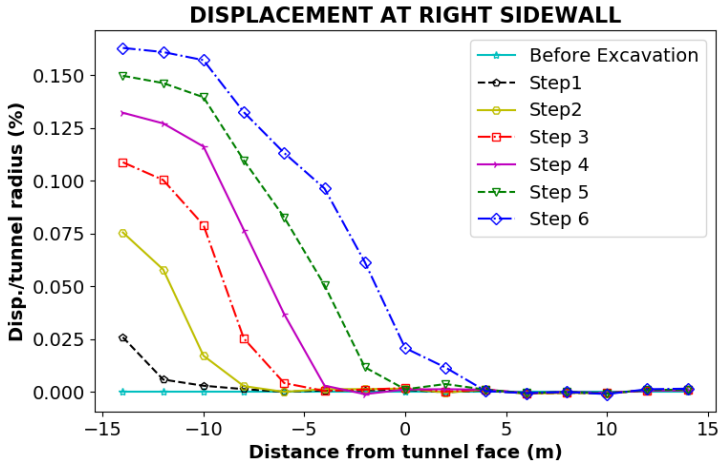

(b)

Figure. 3.5. Displacement along the tunnel during excavation: (a) at the crown; (b) at the right sidewall

Fig. 3.6 and 3.7 show the displacement along the tunnel axis. The effect of the dip angle on the displacement distribution around the tunnel is shown. The displacement mostly distributes at the crown and the invert. At the crown, the displacement extends very far from the tunnel boundary, while it only extends about two tunnel radius from the tunnel boundary at the invert. At the sidewalls, the displacement is much less than that at the crown. It becomes apparent that the displacement zone is limited by pre-existing joints. With dip angles of 0° to 60°, the displacement zone at the crown extends very further from the tunnel boundary. The large displacement mainly distributes at the crown about one tunnel radius. Fig. 3.7 shows the displacement, which is measured along the tunnel at the gauges far from the tunnel boundary of 1 m. The displacement is about 0.25 – 0.37% tunnel radius at the crown, approximately 0.25% tunnel radius at the invert. The

displacement at the sidewalls is very small. Normally, it is less than 0.1% tunnel radius. At the failure positions, the displacement exceeds 0.1% tunnel radius. The displacement is relatively small with dip angles of 75°- 90°. The displacement around the tunnel is approximately 0.2% tunnel radius at the crown and invert, while at the sidewalls, it is less than 0.1% tunnel radius.

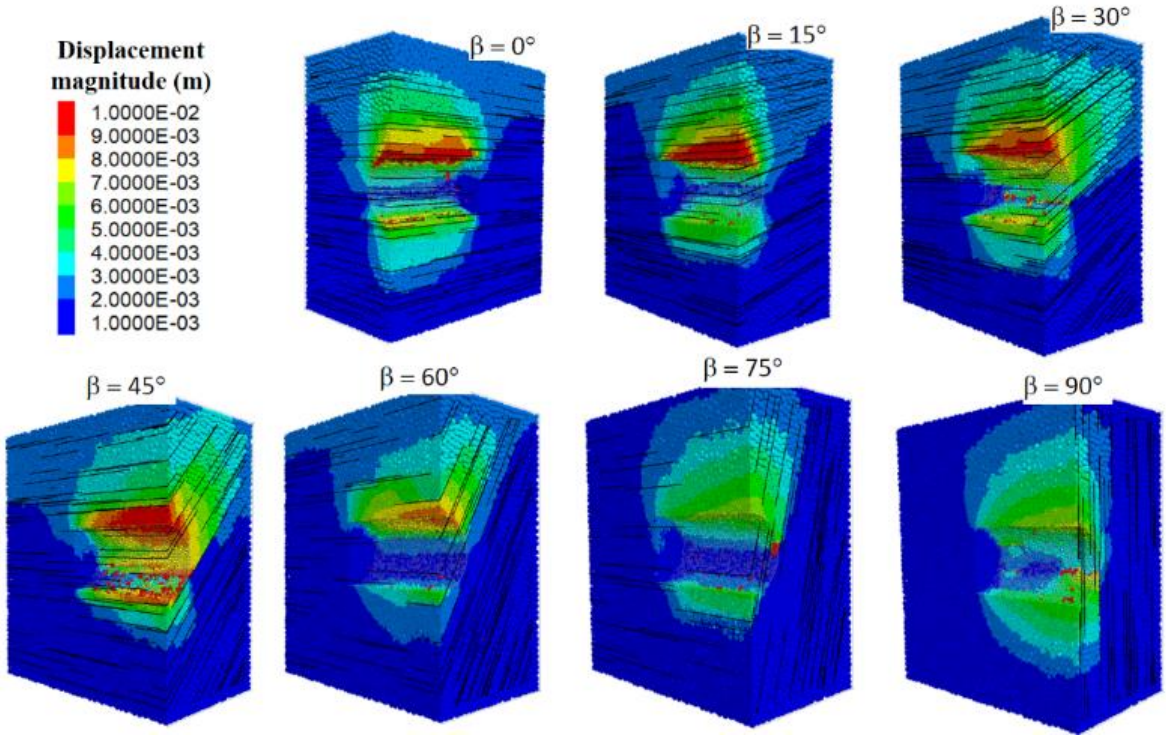

Fig. 3.6. The displacement along the tunnel axis

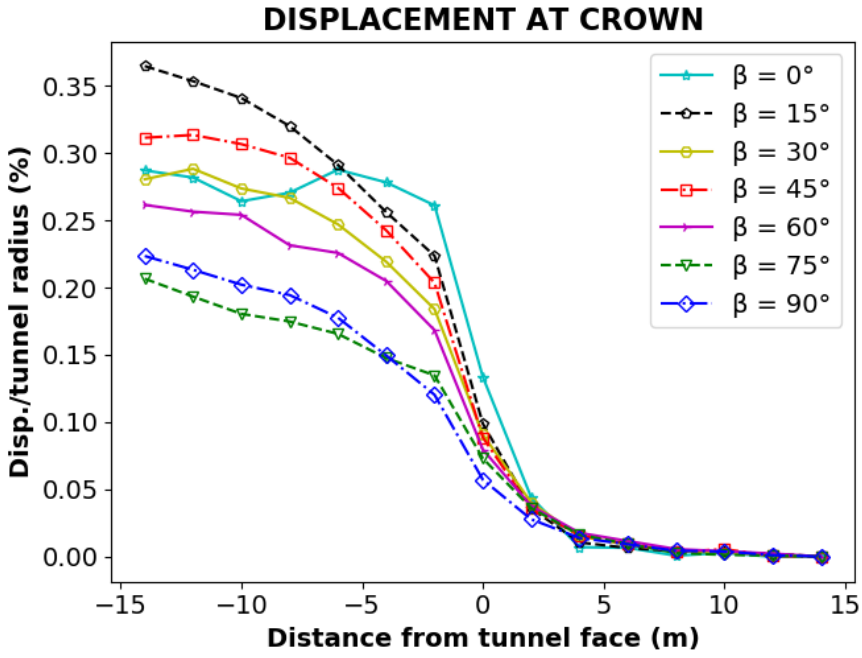

(a)

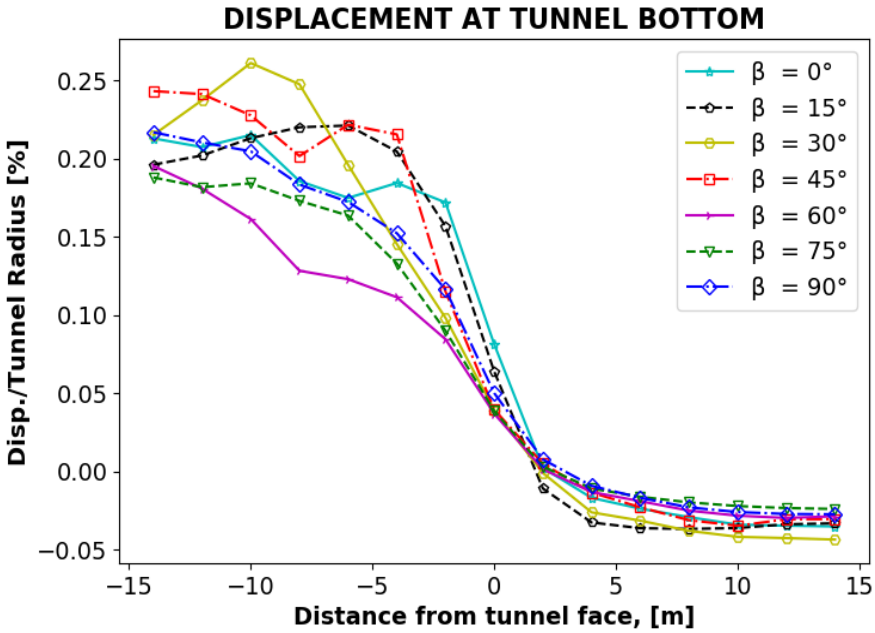
DISPLACEMENT AT TUNNEL BOTTOM
Disp./Tunnel Radius [%]
Distance from tunnel face, [m]
β = 0°
β = 15°
β = 30°
β = 45°
β = 60°
β = 75°
β = 90°

(b)

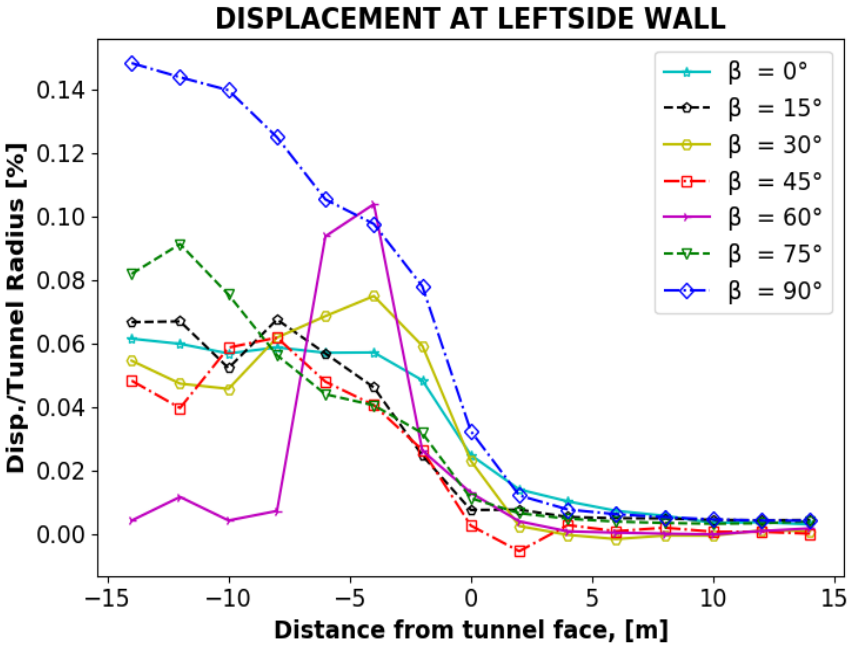
DISPLACEMENT AT LEFTSIDE WALL
Disp./Tunnel Radius [%]
Distance from tunnel face, [m]
β = 0°
β = 15°
β = 30°
β = 45°
β = 60°
β = 75°
β = 90°

(c)

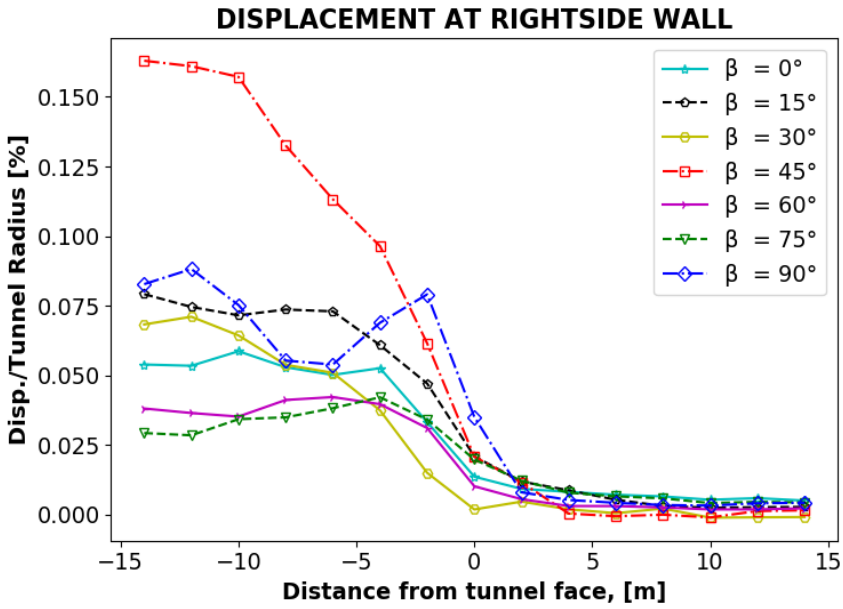

(d)

Fig. 3.7. The displacement along the tunnel axis: (a) at the crown; (c) at the left sidewall, and (d) at the right sidewall

Fig. 3.8 shows the displacement zone at the cross-section C1. The cross-section perpendicular to the tunnel axis explains more clearly the role of the dip angle on the displacement distribution around the tunnel. With low dip angles (i.e., 0°, 15°), the displacement only distributes at the crown and invert. The shapes of the displacement zone at the crown and invert are relatively symmetric. However, the displacement zone at the crown extends very farther from the tunnel boundary. The development tendency of the displacement zone is perpendicular to the joint. The rock mass at the crown is separated by the joints to form the beams. The beams tend to be bent into the tunnel under the overburden pressure. This results in a large displacement at the crown. The displacement around the tunnel at cross-section C1 is shown in Fig. 3.9. The displacement at the crown extends very far from the tunnel boundary, in excess of 3.5 tunnel radius. With high dip angles of 60° - 90°, the displacement is smaller than that of other dip angles. At the invert, the displacement distributes about two tunnel radius, whereas it only distributes near the tunnel boundary at the sidewalls.

With the dip angles of 30° to 45°, the extent of the displacement zone is the strongest. At the crown, the extent of the displacement zone exceeds the 3.5 tunnel radius. The width of the displacement zone dominates compared to that of other dip angles. The displacement zone is the transition from symmetry to asymmetry, as well as the onset

of the development of the displacement along the joints. The displacement zone develops in two directions along the joint and perpendicular the joints, as shown in Fig. 3.8. At the invert, the shape of the displacement zone is relatively symmetric with the dip angle of 30°, whereas with the dip angle of 45° the displacement zone almost develops along the joints. The extent of the displacement zone is limited by the joints. In the direction perpendicular to the joint, the displacement zone develops to a smaller extent. The displacement at the invert only develops and extends along the joints.

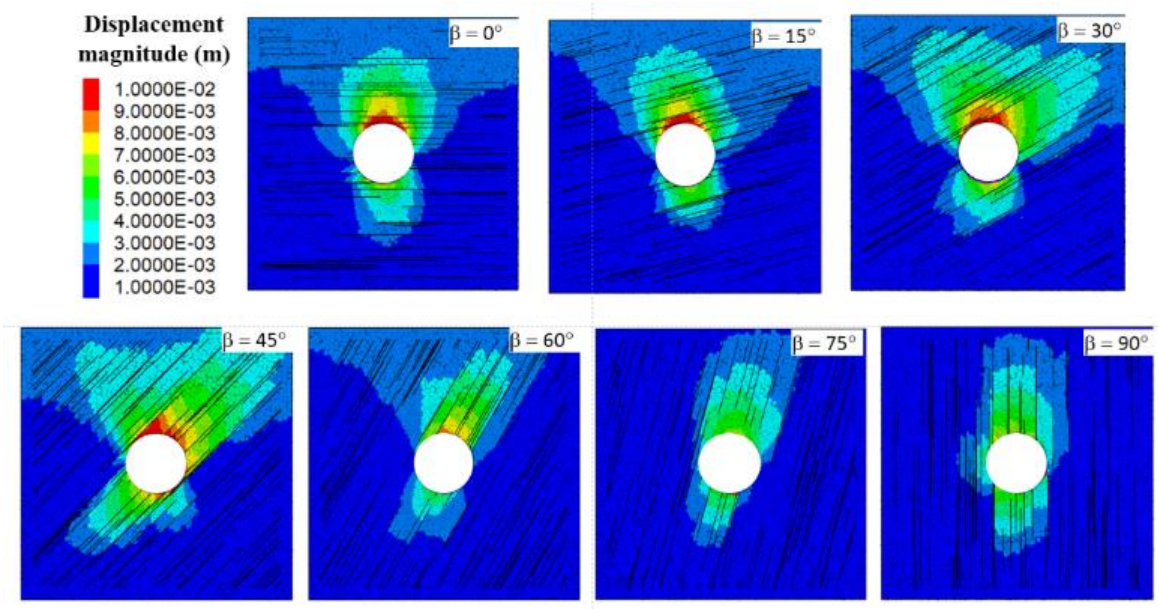

Fig. 3.8. Displacement around the tunnel at the cross-section parallel to tunnel axis

With high dip angles (i.e., 60° and 90°), the displacement is the smallest, as shown in Fig. 3.9a. It only develops along the joints. Fig. 8 shows the strong asymmetry of the displacement zone with high dip angles. The extent of the displacement zone is very narrow and limited by the joints. At the sidewall, several positions showed the large displacement due to the buckling phenomenon.

Besides, the displacement zone at the invert shows the significant government of the dip angle of joints, as illustrated in Fig. 3.8. The displacement zone is relatively symmetric with low dip angles of 0°- 30°, while the displacement zone is strongly asymmetric and narrowly develops along the joint with dip angles of 45°- 90°.

It is clear that the displacement distribution around the tunnel is significantly controlled by the joint dip angle. The displacement zone changes the shape from asymmetry to a strong asymmetry with the increase in joint dip angle. With low dip angles of 0° to 15°, the displacement zone is relatively symmetric at the crown and invert. The displacement

zone expands in two directions: along and perpendicular to the joint with medium dip angles (i.e., 30° – 45°). Finally, with high dip angles of 60°- 90°, the displacement zone only extends along the joints and is limited in the space between the joints at the crown and invert of the tunnel.

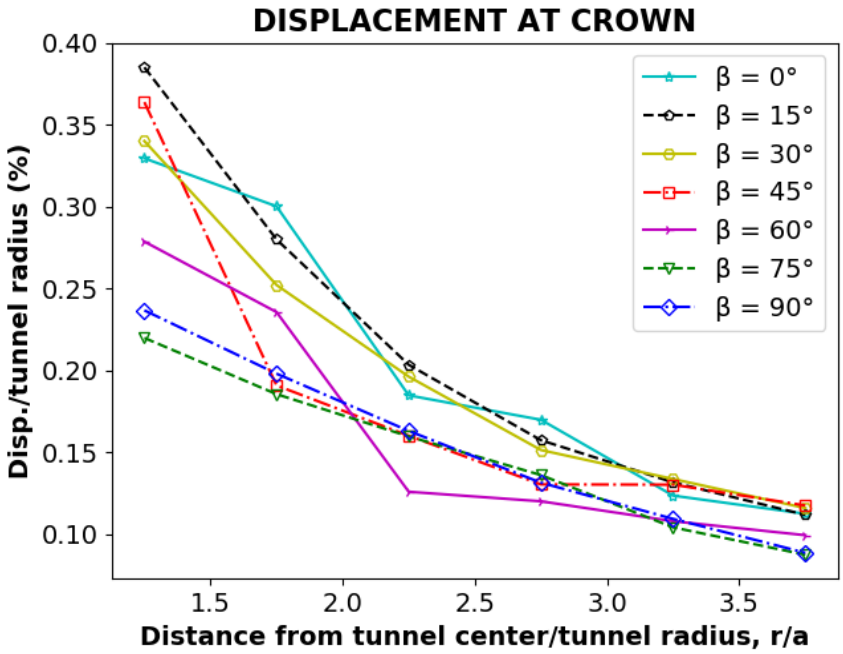

(a)

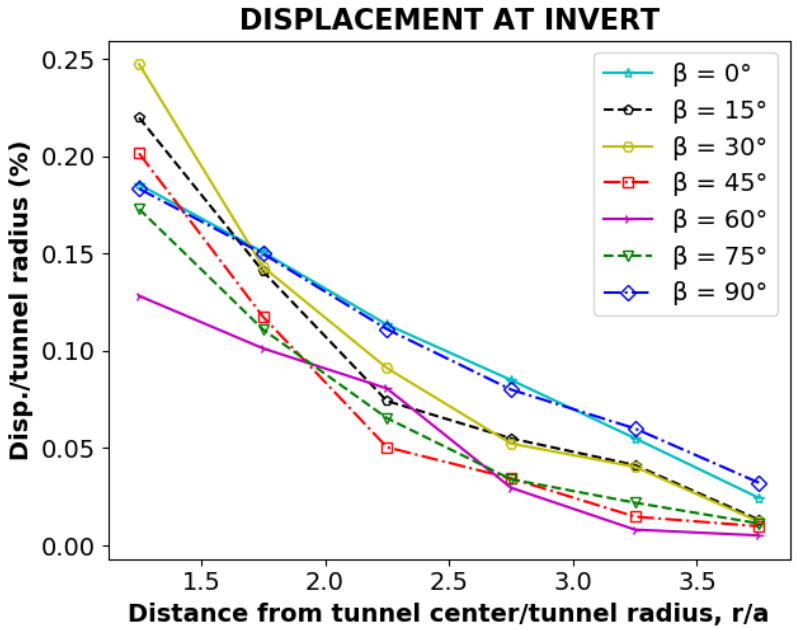

(b)

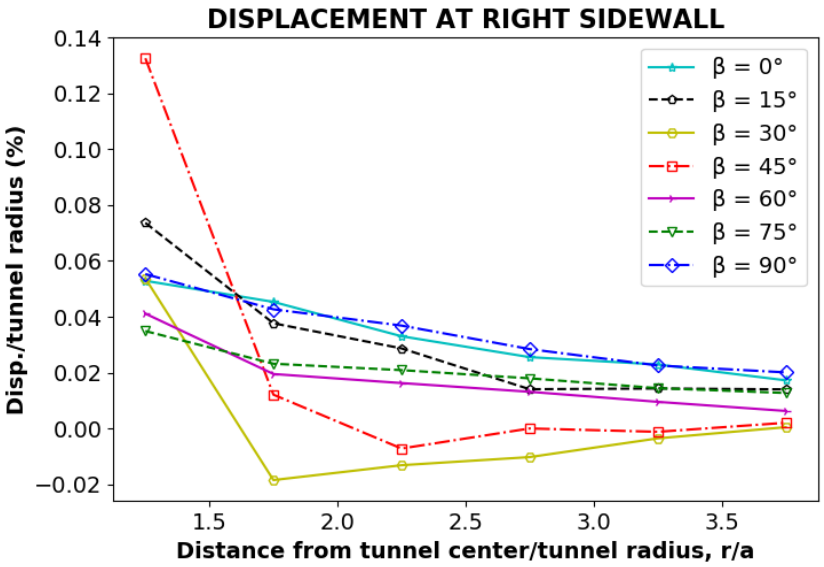

(c)

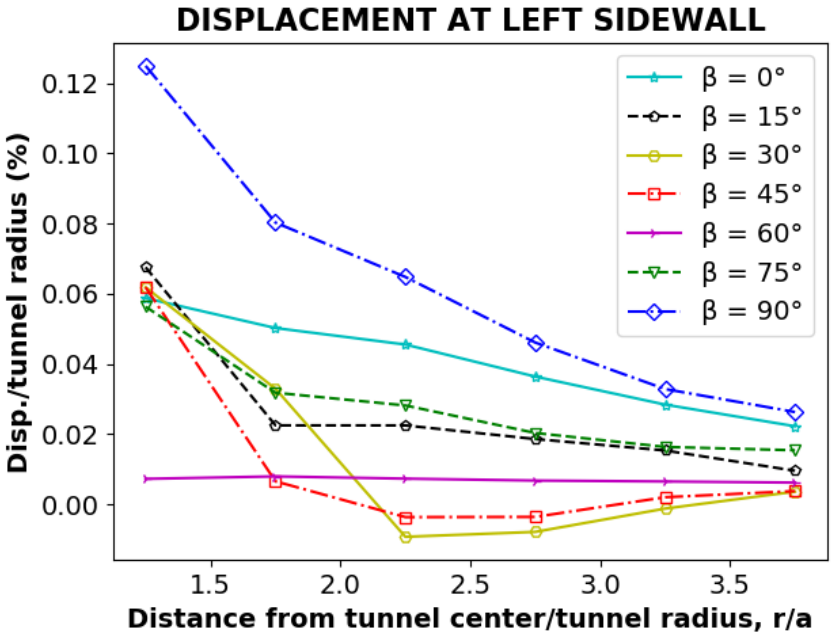

(d)

Fig. 3.9. Displacement at cross-section C1: (a) at the crown, (b) at the invert, (c) at the right sidewall, and (d) at the left sidewall

3.3. Effect of dip angle on the displacement field

The displacement field can be understood as an assemblage of displacement vectors of all particles in a domain that depicts the magnitude and direction of the displacement vector [19]. Fig. 3.10 represents the displacement field in the DEM model, in which the direction and magnitude of displacement are represented by arrow direction and colors, respectively. The arrows depict the movement direction of the particles. The different colors depict the displacement magnitude. The same displacement scale is applied for

all dip angles. The range of color from dark blue to red represents the displacement scale, in which the former represents the minimal displacement, the latter shows the large displacement. To better understand the tendency for rock mass movement concerning pre-existing joints around the tunnel, the displacement field analysis is adopted. From the displacement field, the relative movement direction of particles with pre-existing joints is an important sign to classify the movement types of rock mass around the tunnel. Fig. 3.10 shows the displacement fields of different dip angles. Based on the relative movement of particles with respect to pre-existing joints around the tunnel, four types of the relationship between the movement of particles and pre-existing joints are shown in Fig. 3.11.

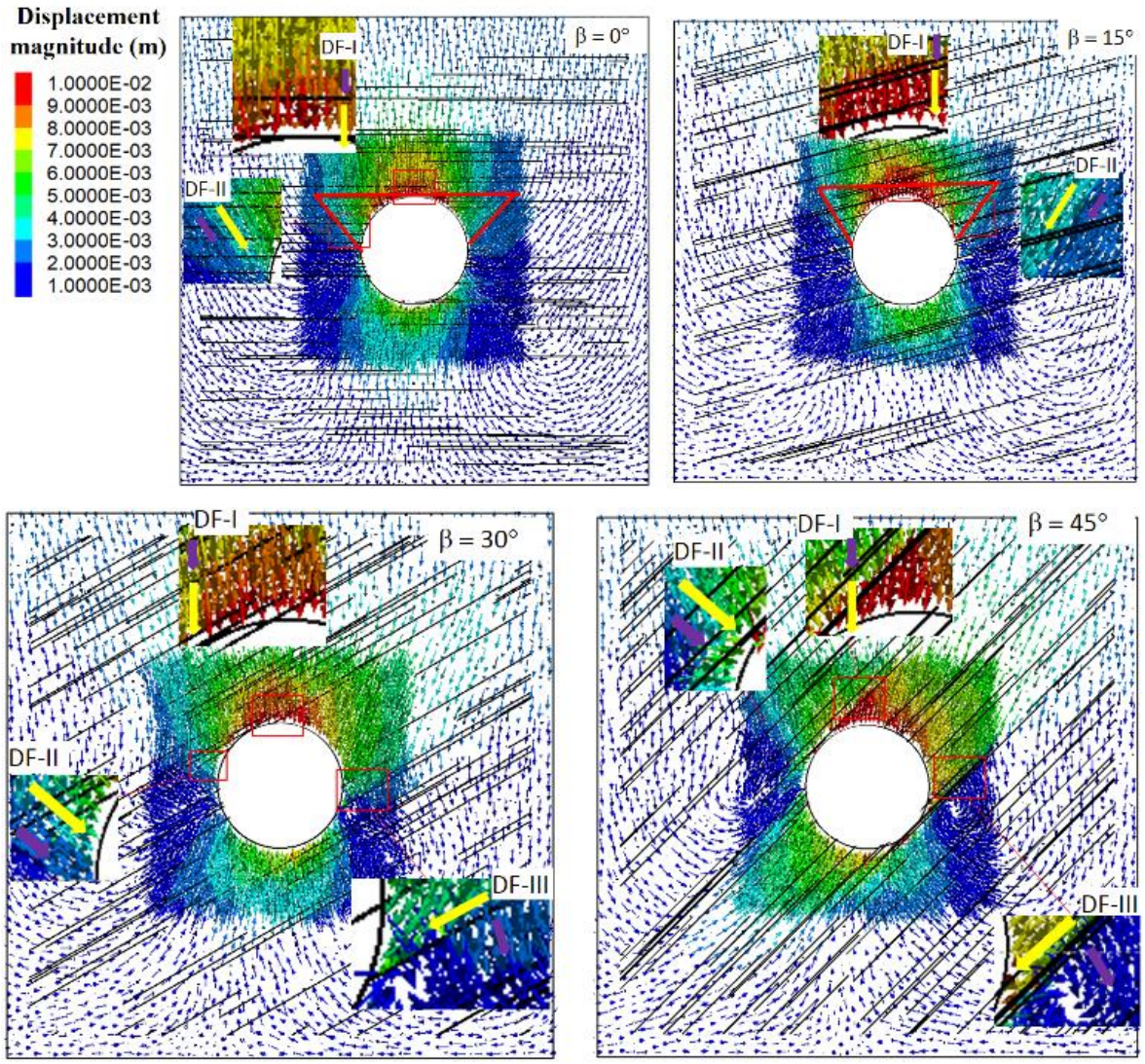

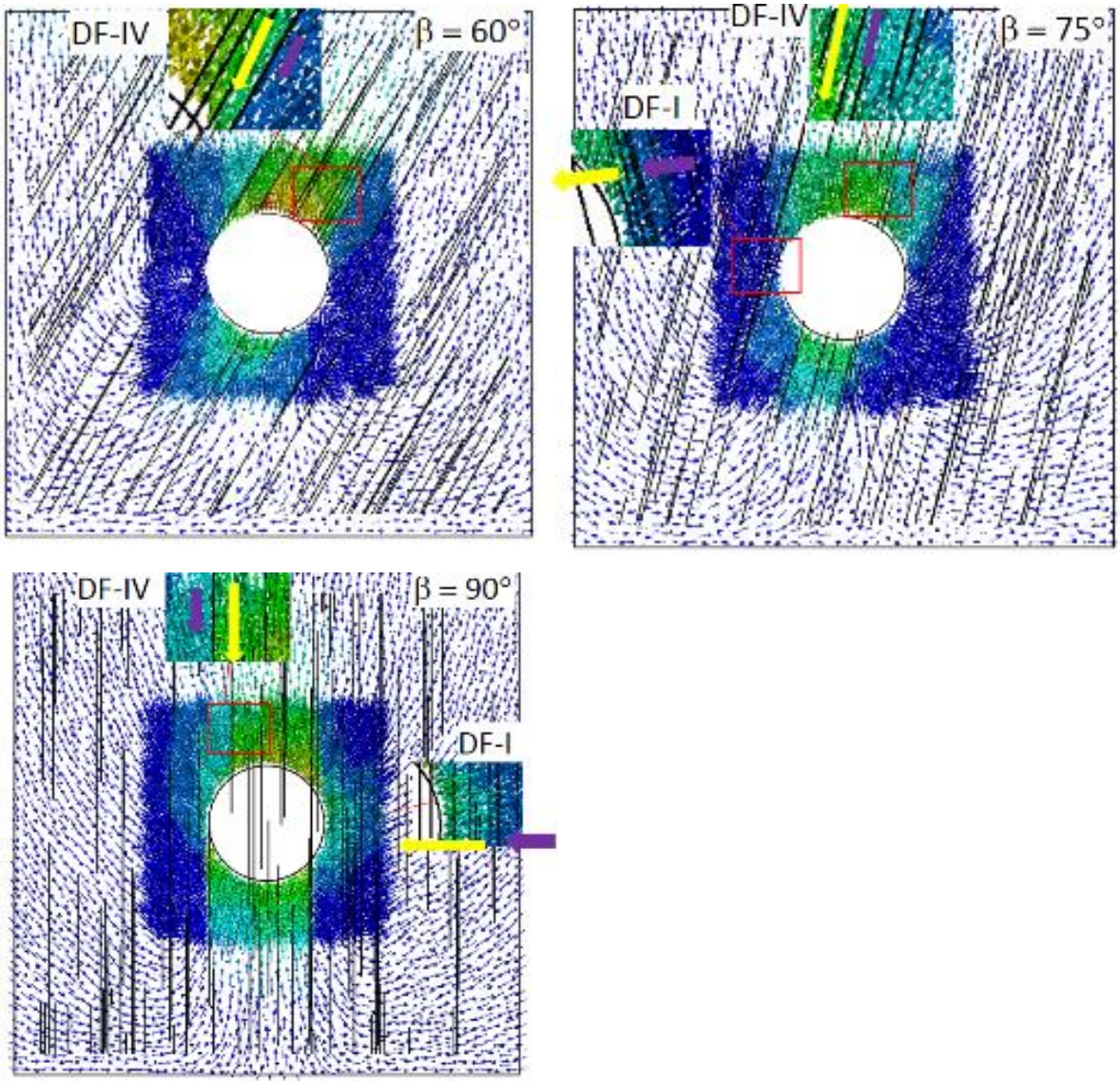

Fig. 3.10. The displacement field with different dip angles

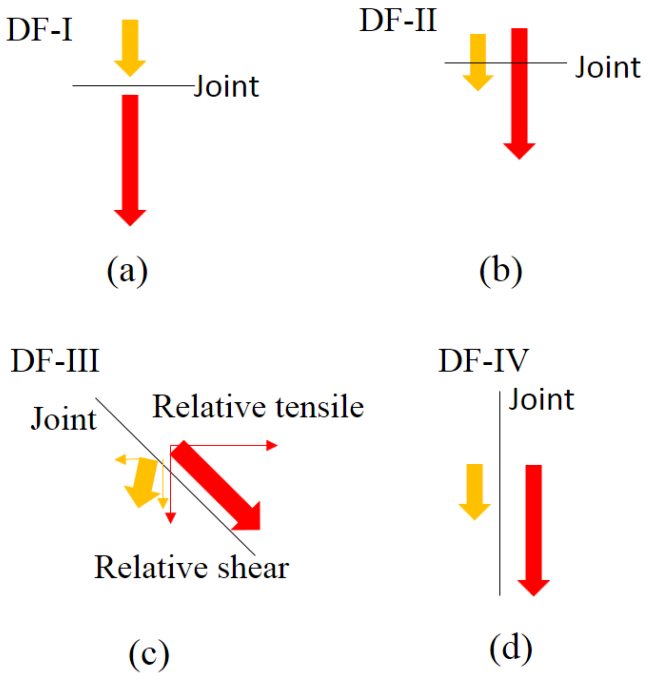

Fig. 3.11. Four displacement field types: (a) Type I – relative tensile displacement field (DF-I); (b) Type II – relative shear displacement field in intact rock (DF-II); (c) Type III – relative shear and tensile displacement field (DF-III); (d) Type IV – relative shear displacement along the joint (DF-IV)

The relative tensile displacement type (DF-I) is depicted by the movement of two-particle sets, in which two particle sets lying on opposite sides of the joints move in the same direction, but their movement rates are different. This type occurs when the joints separate the rock mass into the beams or layers. Due to the effect of excavation, the beams or layers have a tendency to move into the space of the tunnel. The displacement rate of the beams is not similar. The closer the tunnel boundary, the larger the displacement rate. This results in the detachment between the beams. This type normally occurs at the crown with low dip angles (i.e., 0°- 45°), at the shoulder with dip angles (30°- 45°), and the sidewalls with high dip angles (60°- 90°). It is a cause of the spending and buckling failure mode around the tunnel.

The relative shear displacement type in intact rock (DF-II): is described by two sets of particles moving parallel together in a similar direction, but their movement rate is different. This results in the relative shear displacement at the interface between two-particle sets. This type cut through the pre-existing joint. It occurs at both shoulders of the tunnel with dip angles of 0 - 15°, and left shoulder with a dip angle of 30°. This type can cause the shear failure at the shoulders with a failure angle of approximately 45° when rock mass contains the low joint dip angles.

The relative shear and tensile displacement type (DF-III): is characterized by two displacement tendencies representing both a relative shear displacement and relative tensile displacement due to the effect of pre-existing joints. Two particle sets lying on the opposite sides of the joints have a different tendency of movement, in which the particle set lying on the joint moves along the joint into the tunnel, the other lying under the joints tends to move perpendicular to the joints and detaches from the joints. Based on the analysis of the components of displacement vectors, both relative shear and tensile displacements are shown in this type. It occurs at the right sidewall with the dip angle of 30° to 45°.

The relative shear displacement along the joint (DF-IV): is characterized by the two displacement trend lines, which have a similar movement direction along the joints, but

their displacement rate is different. This causes relative shear displacement along the joints. This type occurs at the crown and the invert of the tunnel with high dip angles (i.e., 60°-90°)

Based on the displacement field around the tunnel, we can predict the failure modes. With low dip angles (i.e., 0° -15°), the DF-I and DF-II are dominant. At the crown and invert, the horizontal and near-horizontal joints cut the rock mass into the beams or layers. Under gravity and overburden pressures, the layers or beams will bend and detach from the rock mass into the tunnel space. At the shoulders, the relative shear displacement in intact rock (DF-II) is shown. The sliding mode can occur at the shoulders with the sliding surface cut through the pre-existing joints. The sliding surface is about 45° compared to the vertical direction.

With medium dip angles of 30°- 45°, the four types of displacement fields were observed. The DF-I is shown at the crown and the invert with the dip angle of 30° and only at the crown with the dip angle of 45°. So, the detaching failure mode can occur at these positions. The rock blocks will detach from the rock mass and spall into the tunnel. At the right sidewall, the joint dipping into the tunnel, the DF-III is observed. The rock mass tends to slide the joints into the tunnel. It is clear that the sliding mode can be predicted at the right sidewall. At the left shoulder, the DF-II is observed. The rock blocks can slide into the tunnel due to the coalescence of new shear cracks.

With high dip angles (i.e., 60°- 90°), the DF-IV is predominant. The rock mass can slide along the joints into the tunnel. It is apparent that the sliding failure along the joint is the most important. It can cause serious failure around the tunnel. Otherwise, the DF-I can be observed at the sidewalls. The joint cuts the rock mass at the sidewall into the beams layers. Because of the high-stress concentration at the sidewall, the beams and layers are subjected the uniaxial loading. This results in the layers or beams being bent and broken, called “buckling failure mode.”

4. CONCLUSION

1. The three-dimensional bond-particle discrete element method and smooth joint model were used to create the fractured transversely isotropic rock mass. The mechanical behavior of fractured rock mass and the effect of geometrical fracture parameters (D,

P_{32}, and κ) on the anisotropy of fractured rock mass were investigated. The failure modes of fractured transversely isotropic rock mass could be classified into four types: sliding along the inherent fracture (SL), sliding or split across the inherent fracture (SS), splitting along the inherent fracture (SP), and mixed-mode (M).

The numerical results showed that the relationships between Young's modulus, uniaxial compressive strength, and inclination angles of fractured rock mass exhibited a U-shaped relationship. Specimens containing horizontal and vertical fractures yielded high Young's modulus and uniaxial strength, and modes of failures in these cases were SS and SP. With others, the failure mode was SL, and it exhibited low Young's modulus and uniaxial compressive strength.

2. The construction of the tunnel in the transversely isotropic rock mass always poses a huge challenge due to the strength and elastic anisotropy of the construction media. In this study, the synthetic rock mass generated by PFC3D succeeded in simulating the mechanical behavior of the transversely isotropic rock mass. Moreover, the effect of joint dip angle on the displacement distribution around the tunnel in tunneling was studied. The displacement only distributed at the crown and invert the tunnel. At the sidewall, the displacement is relatively small. With low dip angles of 0° - 15°, The shapes of the displacement zone at the crown and invert are relatively symmetric. The extent of displacement zone at the crown exceeds 3.5 tunnel radius, while it is about two tunnel radius at the invert. With medium dip angles of 30°- 45°, the shapes of the displacement zone are the transition from symmetry to asymmetry. The displacement at the crown develops in two directions. One direction is parallel to the joints, whereas the other is perpendicular to the joint. The extent of the displacement zone at the crown extends very far from the tunnel boundary and reaches the boundary of the model. With high dip angles (i.e., 60° - 90°), the displacement at the crown and invert is the smallest. The displacement zone distributes along the joints. The extent of the displacement zone is strongly governed by the joints.

3. Four types of displacement field, such as relative tensile (DF-I), relative shear in intact rock (DF-II), relative shear and tensile (DF-III), and relative shear along the joint (DF-IV) were shown. The DF-I has a tendency to cause detaching and buckling failure. It is observed at the crown with low dip angles, at the left sidewall with medium dip angles, and at the sidewalls with high dip angles. The DF-II is observed at the shoulders with

the low dip angles and the left shoulder with medium dip angles. It can result in forming new shear cracks. The DF-III is seen at the right sidewall with the medium dip angles. The rock mass tends to slide along the joint into the tunnel. Finally, the DF-IV is seen at the crown and right shoulder with high dip angles. The rock mass slide along the joints into the tunnel.

REFERENCE

1. Bui, Van-Binh. *Effect of Excavation Direction on Stability of Tunnels in Transversely Isotropic Rock Mass*. 2022. PhD Thesis. National Central University.
2. Bui, Van-Binh, et al. "FAILURE MODES OF CIRCULAR TUNNELS IN A TRANSVERSELY ISOTROPIC ROCK MASS." *Journal of GeoEngineering* 17.1 (2022): 33-46.
3. Bui, V. B., Tien, Y. M., & Juang, C. H. (2021, June). Numerical Simulation of Effect of Joint Dip Angle on Displacement Around the Tunnel. In *55th US Rock Mechanics/Geomechanics Symposium*. OnePetro.
4. Tien, Y. M., Bui, V. B., Liu, C. H., & Juang, C. H. (2020, June). Numerical modeling of mechanical behaviors of fractured transversely isotropic rock masses. In *54th US Rock Mechanics/Geomechanics Symposium*. OnePetro.